HHS Public Access

Author manuscript

Sci Transl Med. Author manuscript; available in PMC 2017 November 17.

Published in final edited form as:

Sci Transl Med. 2017 May 17; 9(390): . doi:10.1126/scitranslmed.aal3128.

In situ bone tissue engineering via ultrasound-mediated gene delivery to endogenous progenitor cells in mini-pigs

Maxim Bez[1,2], **Dmitriy Sheyn**[2,3], **Wafa Tawackoli**[2,3,4,5], **Pablo Avalos**[3], **Galina Shapiro**[1], **Joseph C. Giaconi**[6], **Xiaoyu Da**[4], **Shiran Ben David**[2,3], **Jayne Gavrity**[7], **Hani A. Awad**[7], **Hyun W. Bae**[2], **Eric J. Ley**[2], **Thomas J. Kremen**[2,8], **Zulma Gazit**[1,2,3,8], **Katherine W. Ferrara**[9], **Gadi Pelled**[1,2,3,4,5,*], and **Dan Gazit**[1,2,3,4,5,8,*,†]

[1]Skeletal Biotech Laboratory, Hadassah Faculty of Dental Medicine, The Hebrew University of Jerusalem, Ein Kerem, Jerusalem 91120, Israel

[2]Department of Surgery, Cedars-Sinai Medical Center, 8700 Beverly Boulevard, Los Angeles, CA 90048, USA

[3]Board of Governors Regenerative Medicine Institute, Cedars-Sinai Medical Center, Los Angeles, CA 90048, USA

[4]Biomedical Imaging Research Institute, Cedars-Sinai Medical Center, Los Angeles, CA 90048, USA

[5]Department of Biomedical Sciences, Cedars-Sinai Medical Center, Los Angeles, CA 90048, USA

[6]Department of Imaging, Cedars-Sinai Medical Center, Los Angeles, CA 90048, USA

[7]Department of Biomedical Engineering and the Center for Musculoskeletal Research, University of Rochester Medical Center, Rochester, NY 14642, USA

[8]Department of Orthopedics, Cedars-Sinai Medical Center, Los Angeles, CA 90048, USA

[†]Corresponding author. dan.gazit@csmc.edu.
[*]These authors contributed equally to this work.

Author contributions: G.P., Z.G., E.J.L., K.W.F., and D.G. contributed to the concept of the study and revised the manuscript. G.P., M.B., and D.G. designed the experiments. M.B., W.T., P.A., T.J.K., and H.W.B. performed large-animal surgical procedures. M.B., D.S., W.T., and J.C.G. performed ultrasound-mediated gene delivery experiments. M.B., D.S., and W.T. extracted bone and soft tissue samples. M.B., D.S., and S.B.D. performed flow cytometry data analysis. S.B.D. performed RT-PCR and ELISA assays. J.G. and H.A.A. performed biomechanics testing. M.B. and G.S. performed the statistical analyses. M.B., W.T., and X.D. performed μCT imaging and biomechanical data analysis. M.B., G.S., and G.P. wrote the manuscript.

Competing interests: T.J.K., G.P., and D.G. are inventors on patent application (PCT/US2017/020033) submitted by Cedars-Sinai Medical Center that "covers the use of ultrasound for endogenous stem cell activation." G.P., Z.G., and D.G. are shareholders in GamlaStem Medical Inc., which did not provide funds for this study. All other authors declare that they have no competing interests.

Data and materials availability: All materials are available from commercial sources or can be derived using methods described in this study. All relevant data are reported in the article.

SUPPLEMENTARY MATERIALS

www.sciencetranslationalmedicine.org/cgi/content/full/9/390/eaal3128/DC1

Fig. S1. Critical-sized bone fracture model in Yucatán mini-pigs' tibia.
Fig. S2. Endogenous mesenchymal progenitor cell recruitment to mini-pig tibial fracture site.
Fig. S3. Ultrasound treatment setup.
Fig. S4. Biodistribution of *BMP-6* expression after ultrasound-mediated gene delivery.
Fig. S5. Comparison of bone formation between male and female mini-pigs.
Table S1. Primary data.
Data file S1. MATLAB code of biomechanical analysis.

[9]Department of Biomedical Engineering, University of California, Davis, 451 Health Sciences Drive, Davis, CA 95616, USA

Abstract

More than 2 million bone-grafting procedures are performed each year using autografts or allografts. However, both options carry disadvantages, and there remains a clear medical need for the development of new therapies for massive bone loss and fracture nonunions. We hypothesized that localized ultrasound-mediated, microbubble-enhanced therapeutic gene delivery to endogenous stem cells would induce efficient bone regeneration and fracture repair. To test this hypothesis, we surgically created a critical-sized bone fracture in the tibiae of Yucatán mini-pigs, a clinically relevant large animal model. A collagen scaffold was implanted in the fracture to facilitate recruitment of endogenous mesenchymal stem/progenitor cells (MSCs) into the fracture site. Two weeks later, transcutaneous ultrasound-mediated reporter gene delivery successfully transfected 40% of cells at the fracture site, and flow cytometry showed that 80% of the transfected cells expressed MSC markers. Human *bone morphogenetic protein-6* (*BMP-6*) plasmid DNA was delivered using ultrasound in the same animal model, leading to transient expression and secretion of BMP-6 localized to the fracture area. Micro–computed tomography and biomechanical analyses showed that ultrasound-mediated *BMP-6* gene delivery led to complete radiographic and functional fracture healing in all animals 6 weeks after treatment, whereas nonunion was evident in control animals. Collectively, these findings demonstrate that ultrasound-mediated gene delivery to endogenous mesenchy-mal progenitor cells can effectively treat nonhealing bone fractures in large animals, thereby addressing a major orthopedic unmet need and offering new possibilities for clinical translation.

INTRODUCTION

Fracture nonunion, when the normal process of fracture repair is thwarted and the fracture fails to heal, constitutes a complex medical condition with an estimated incidence of 100,000 new nonunion cases every year in the Unites States alone (1). These injuries not only cause patients to suffer but also lead to long-term hospitalization and disability, repeated surgeries, loss of working days, and considerable costs to the health system (2). Various factors affect the incidence of nonunion formation, including fracture pattern, anatomical location, degree of bone loss, and the quality of surgical treatment (3).

Currently, the gold-standard treatment for fracture nonunion is autologous bone grafting (autografts). However, autografts are not always available and their harvest often leads to prolonged postoperative pain and substantial donor site morbidity (4). Bone allografts are readily available from tissue banks and, therefore, are an alternative to autografts. Unfortunately, allografts have very low osteogenic potential, leading to poor graft-host integration that results in numerous failures due to fractures and nonunion (5). In recent years, recombinant human bone morphogenetic proteins (BMPs) have been introduced to the clinic, among other indications, for long-bone fracture repair. Local administration of BMP-2 (6) and BMP-7 (7) in patients with tibial nonunions resulted in increased healing rates. However, BMPs are costly and have been associated with a high incidence of side effects including infection, heterotopic bone formation, and immunogenic reactions,

possibly due to their use in megadoses (8). Thus, fracture nonunion remains a clear unmet clinical need.

An attractive alternative to BMP protein therapy is a local targeted gene therapy (9). Such therapy could facilitate nonunion healing via transient overexpression of an osteogenic *BMP* gene without requiring the production of high-cost recombinant proteins or their administration in megadoses. Viral *BMP* gene delivery has been shown to induce nonunion healing in rodents and large animals (10–12). Although viral vectors are considered to be efficient gene delivery methods, they introduce risks of malignancy and immunogenic reactions, which greatly limits their translational potential (13). Nonviral vectors are considered safer for human use, albeit much less efficient for gene expression (9). Our group showed that in vivo electroporation of a *BMP* gene to endogenous mesenchymal stem cells (MSCs) within a nonunion fracture site yielded efficient fracture healing in rodents (14). Although successful, this approach requires the insertion of electrodes and conduction of powerful electrical currents resulting in pain and tissue damage, limiting its use in clinical applications.

An alternative physical method of gene transfection, sonoporation—the use of ultrasound for gene delivery—is especially attractive (15). Ultrasound is widely used in medicine and considered one of the safest imaging modalities. In addition, ultrasound can be applied noninvasively to many different regions of interest and can reach deep-lying tissues with minimal systemic side effects. Sonoporation uses ultrasonic waves to increase cell membrane permeability by forming transient nanosized pores in the membrane, subsequently enhancing uptake of drugs and nucleic acids (16–18). Most studies have combined ultrasound with the administration of formulated microbubble suspensions to enhance the delivery of nucleic acids to target cells (19–23). Such micro-bubble suspensions contain micrometer-sized bubbles filled with a low-diffusivity gas core and stabilized by a shell. Originally designed and U.S. Food and Drug Administration–approved for use as blood pool contrast agents, exposure to ultrasound drives microbubbles to a forced oscillation state in which the gas core is repeatedly compressed and expanded. Within a range of ultrasound parameters, these microbubbles can deform the cell membrane and form membrane pores, thus enhancing the cellular uptake of drugs and nucleic acids.

Recently, we showed that the combination of ultrasound and microbubbles can be used to overexpress a reporter gene in endogenous MSCs recruited to a fracture site in a large animal model (24). Although ultrasound-mediated *BMP* gene delivery was shown to induce ectopic bone formation in vivo (25–27), previous attempts at fracture repair were not successful (25). Here, we hypothesized that microbubble-enhanced, ultrasound-mediated gene delivery of a *BMP* gene would lead to efficient bone regeneration and fracture healing in a clinically relevant, large animal model (porcine). Multiple structural, biomechanical, and safety parameters were monitored to demonstrate the feasibility of this therapeutic approach for human use.

RESULTS

Sonoporation leads to reporter gene expression in endogenous MSCs recruited to fracture site

Mini-pigs underwent surgery during which a 1-cm critical-sized tibial bone fracture was created, a biodegradable collagen scaffold was implanted, and fractures were internally fixated with custom-made dynamic compression plates (fig. S1). The fracture sites were treated with microbubble-enhanced, ultrasound-mediated gene delivery 14 days after surgery, when maximal cell recruitment of mesenchymal lineage was noted (fig. S2). Plasmid DNA encoding a reporter gene [*green fluorescent protein* (*GFP*) or *luciferase*] mixed with microbubbles was transcutaneously injected into the fracture site, and half of the animals were randomly assigned to receive ultrasound treatment (fig. S3). Ex vivo optical imaging of the fracture site revealed fluorescent signal localized to the fracture site in *GFP*-treated animals (Fig. 1A). Flow cytometry revealed that 40% of cells collected from within the tibial fracture of animals treated with ultrasound (US) expressed GFP six times greater than that observed in untreated animals (No US, $P = 0.049$; Fig. 1B). GFP-expressing cells from bone fractures in ultrasound-treated animals were also three times more fluorescent ($P = 0.0013$; Fig. 1C). In another experiment, cells isolated from bone fractures in animals treated with *luciferase* and ultrasound demonstrated 80 times more luciferase activity than cells from fracture sites in animals not subjected to ultrasound ($P = 0.0001$; Fig. 1D). An examination of the transfected cells showed significantly more cells expressing MSC markers CD29 and CD90 in the ultrasound-treated group: 90% of GFP-positive cells in the ultrasound-treated group were CD29-positive and 80% of GFP-positive cells were CD90-positive, whereas only 30% of GFP-positive cells in the untreated group were CD29-positive ($P = 0.0001$; Fig. 1E) and 40% were CD90-positive ($P = 0.0057$; Fig. 1F). No significant differences were observed in CD44-positive cells, a cell marker of mesenchymal lineage ($P = 0.0531$; Fig. 1G). Overall, ultrasound-treated fracture sites exhibited significantly higher progenitor transfection rates and stronger transgene expression.

Sonoporation induces transient *BMP-6* expression at bone fracture site

Eighteen pigs received tibial fractures as described above and were treated with ultrasound after local injection of *BMP-6* and microbubbles (*BMP-6* + US) or injection of *BMP-6* and microbubbles without ultrasound application (*BMP-6* control). Local expression of *BMP-6* gene after sonoporation to tibial bone fractures was evaluated over time. Quantitative polymerase chain reaction (PCR) analysis of isolated cells from the fracture site showed 850- and 400-fold higher *BMP-6* expression in ultrasound-treated animals compared to control animals on days 2 and 5 after treatment, respectively (Fig. 2A). On day 10, *BMP-6* gene expression was undetectable. Similarly, BMP-6 protein secretion in the fracture site was 70- and 120-fold higher on days 2 and 5 after treatment, respectively, compared to animals that were not treated with ultrasound (Fig. 2B). Negligible amount of BMP-6 protein was detected on day 10. In addition, no overexpression of *BMP-6* was found in off-target tissues (fig. S4).

BMP-6 sonoporation facilitates in vivo bone regeneration

Next, the therapeutic effect of local *BMP-6* gene delivery was evaluated in the same pig model of tibial nonhealing fracture. Tibial fracture regeneration in *BMP-6* + US–treated animals was compared to a nontreated control group (Scaffold only), animals treated with plasmid premixed with microbubbles without ultrasound (*BMP-6* only) or an empty plasmid premixed with microbubbles and ultrasound (US only), and a gold-standard control group treated with an autograft (Autograft). Micro–computed tomography (μCT) analysis 8 weeks after surgery revealed that fractures treated with *BMP-6* + US regenerated 75% of their volume with new-formed bone, which was equivalent to autograft transplantation ($P = 0.102$) and doubled the bone volume density seen in all other treatment groups ($P = 0.0001$; Fig. 3A). No differences in healing were noted between male and female pigs within the *BMP-6* + US group ($P = 0.3945$; fig. S5). In addition, the new-formed bone in the *BMP-6* + US group was significantly more calcified than in all other groups ($P = 0.0029$; Fig. 3B) except the Autograft group ($P = 0.068$). Only fractures treated with *BMP-6* + US or autograft showed union, evident by the complete cortical continuity of the tibia (Fig. 3C). Histological analysis showed that there was a complete regeneration of the fracture with mature new-formed bone and the presence of osteocytes in *BMP-6* + US–treated pigs (Fig. 3D). All other groups showed evidence of insufficient bone formation, abundant granulation tissue deposition, and fibrosis (Fig. 3D).

BMP-6 gene delivery induces functional healing of treated bones

Torsional testing was performed blindly on tibiae excised from the operated animals to examine the mechanical properties of the treated bones 8 weeks after surgery. In accordance with the μCT and histological analysis results, tibial bones from the *BMP-6* + US group showed at least twofold higher mechanical stiffness ($P = 0.02$), strength ($P = 0.0048$), and toughness compared with tibial fractures from the *BMP-6*–only group ($P = 0.0077$; Fig. 4). No significant differences were observed between the *BMP-6* + US and the Autograft groups ($P = 0.1552$).

DISCUSSION

Here, we used ultrasound-mediated, microbubble-enhanced gene delivery for in situ bone engineering in a mini-pig model of tibial fracture repair. We showed that ultrasound-mediated *BMP-6* delivery to cells residing within the fracture site achieved transient local gene expression, mainly targeting endogenous MSCs. Osteogenic gene delivery resulted in a spatial and temporal expression pattern that is consistent with nonviral gene delivery systems. Furthermore, it resulted in complete fracture union within 8 weeks with autograft-equivalent biomechanical properties. No evidence of ectopic transgene expression or inflammatory response was observed, suggesting a favorable safety profile. Using a clinical ultrasound system within the range of parameters used in B-mode ultrasound imaging of microbubble contrast agent in humans, we saw no clinical or histological signs of heating or heat-associated damage.

Almost 20 years ago, Bonadio *et al.* (28) showed for the first time that nonviral gene delivery can achieve complete fracture repair in a large animal model (canine). Using gene-

activated matrix implants containing plasmid DNA encoding human parathyroid hormone, complete critical-sized tibial fracture repair was achieved by 18 and 8 weeks for 1.6- and 1.0-cm-sized fractures, respectively. Since then, other works involving large animals focused mainly on viral gene delivery. Egermann *et al.* (29) showed improved fracture repair after *BMP-2* adenoviral gene delivery in a tibial fracture in osteoporotic sheep. Dai *et al.* (30) showed improved fracture repair after implantation of *BMP-2* virally transduced bone marrow–derived MSCs into a goat tibial fracture. Despite these promising results, viruses have many safety concerns, limiting their use in humans. Xu *et al.* (31) showed that adenoviral *BMP-2* gene delivery to a fracture site resulted in temporary cellular and persistent humoral immune responses against the viral vector. In addition, clinical trials have shown that viral gene delivery can evoke a systemic inflammatory response resulting in death (32) and may cause carcinogenesis by random gene insertions into the genome (33, 34). Thus, efficient nonviral gene delivery methods must be developed for clinical use.

Ultrasound-mediated *BMP* gene delivery had not been successfully applied for fracture repair previously. This is not to be mistaken with low-intensity pulsed ultrasound, which uses different ultrasound parameters, and is applied daily over a period of weeks to the fracture site (35). Feichtinger *et al.* (25) used microbubble-enhanced, ultrasound-mediated gene delivery of *BMP-2* and *BMP-7* in a femur nonunion model in rats. Despite successfully inducing gene overexpression and ectopic bone formation using repetitive treatments, they could not induce significant orthotopic bone formation in a fracture site. These differences can be attributed to diminished osteogenic potentials of BMP-2 and BMP-7 within the fracture site microenvironment, as reported in other animal and clinical studies (36–41). The biological response to BMPs is dependent on the cell type and microenvironment that is present at the site of *BMP* delivery (42–44). BMP-6 has a distinct BMP receptor type 1A specificity, making it less affected by endogenous BMP inhibitors while strongly promoting osteogenesis by osteoblasts (45, 46). Previously, we showed that BMP-6 has better osteogenic potential and induced more efficient bone formation than BMP-2 in vitro and in vivo when overexpressed in MSCs (47). Some studies have suggested that BMP-6 signaling works through mechanisms of both osteochondral and intramembranous ossifications, with the latter being the primary pathway, thus resulting in more rapid calcification within the fracture site (44). Therefore, BMP-6 could serve as a more potent orthotopic bone inducer.

In contrast to the study conducted by Feichtinger *et al.*, our study used a two-step procedure that included recruitment of endogenous progenitor cells to the fracture site. We showed that by implanting a collagen scaffold into the fracture site, efficient endogenous progenitor migration and retention in the scaffold could be achieved within 14 days. Betz *et al.* (10) showed that delayed administration of a *BMP-2*–encoding adenoviral vector improved bone formation in a critical-sized femoral fracture in rats. It is likely that delayed treatment allows for more progenitors to populate the fracture site, making the vector more efficient in targeting cells that respond to BMP secretion and induce bone regeneration. Overall, it seems that the combination of a potent osteogenic protein together with an effective delivery strategy to a viable progenitor population is key to efficient fracture repair.

A modification of the method described here could include preloading of microbubbles and plasmid into the scaffold, which would eliminate the need to inject these materials in a

subsequent procedure. A recent study applied ultrasound to intramuscularly implanted fibrin/ collagen hybrid matrices containing micro-bubbles, *BMP-2*/*7* coexpression plasmids, and C2C12 cells in mice (48). Although that study combined exogenous cells within the scaffold, only a small amount of new bone was generated in vivo. In our two-step method, the recruitment of endogenous progenitor cells is an important factor that occurs over the course of at least 2 weeks, as we have previously shown in rodents (14, 24). Hence, implanting scaffolds containing plasmids and micro-bubbles would require long-term protection of these components because naked DNA is degraded by deoxyribonucleases, and microbubbles have a short half-life of about 10 min when injected locally. To the best of our knowledge, there are technological barriers that still need to be overcome to generate such a composite scaffold. However, local injection, as applied here, is attractive for near-term studies because the properties can be well controlled and injections can be repeated and monitored as needed.

The clinical gold standard for non-union treatment uses autografts (49). As a living tissue, their osteoinductive and osteoconductive properties make them far superior over other types of grafts (50). The most common donor site for bone grafting is the patient's own iliac crest. Because the autografts used here were the native osteotomized tibiae, they were far superior to autografts available in a clinical setting. This autograft group represents a hypothetically perfect case scenario, in which an exact autologous replica of the lost bone was implanted within the fracture site. The autografts used in this study were structurally identical to the fractured site in size, shape, and bone content. This allowed efficient bone formation and complete bridging of the defect in 8 weeks, as seen in our results. In addition, their harvest did not result in donor-site morbidities, shortening the surgical time and improving recovery. Moreover, these autografts were attached to a periosteal blood supply. These factors were shown to improve fracture healing (51, 52). Runyan *et al.* (53) showed that this approach resulted in superior fracture repair relative to other types of grafts. The similarities found between the Autograft and the *BMP-6* + US groups serve as a proof of concept that our proposed therapy is as efficient as an "optimal" autograft for the treatment of critical-sized fractures.

A final difference between our study and that of Feichtinger *et al.* is the use of ultrasound imaging to monitor microbubble oscillation during treatment. This is a key aspect of the protocol because, although ultrasound therapy is highly promising, ultrasound wave propagation is limited by tissue properties. Both bone and fixation plates are highly reflective of ultrasound waves. These reflections can significantly alter the ultrasound field in the fracture site to lower transfection efficacy. This effect was observed in other works, requiring longer ultrasound exposure time for effective gene delivery (54). For efficient gene delivery using our proposed therapy, imaging provides the opportunity to ensure sufficient sonoporation despite the fixation plates that have the potential to impede the ultrasonic waves. More robust ultrasound systems can be implemented to bypass these hurdles in future human therapies (55).

One of the parameters not tested in this study is the use of repeated treatments. Because of the therapy's relative ease and low invasiveness, repeated treatments at various time points might further enhance the effect of osteogenesis and promote faster and improved bone

repair. Thus, implementation of multiple treatments could be another approach in future ultrasound-mediated gene delivery studies. However, note that prolonged ultrasound exposure could result in a variety of adverse effects, including excessive tissue heating and dystrophic calcifications due to tissue damage (22). Using higher ultrasound intensities, the combination of ultrasound and microbubbles can also result in cellular lysis due to jetting during microbubble collapse within the tissue (56).

The current study evaluated the effect of ultrasound-based *BMP* gene delivery for a short term. A long-term study is required to fully assess the efficiency of the method in bone healing compared to controls. Here, all animals received collagen scaffold implants that have been previously shown to have some osteoconductive properties (14, 57). However, even with the inclusion of the scaffold, and within a short period of time, we were able to show significantly higher union rate, bone formation, and biomechanical properties among BMP-6 and ultrasound–treated animals. We can conclude that the combined therapy of a collagen scaffold, *BMP-6* plasmid, microbubbles, and ultrasound is superior to the control groups and is similar to autograft-treated animals.

These results show great promise for future ultrasound-mediated gene therapies to tissues. Because ultrasound technology is safe and widely used in the clinic, this approach can easily be translated into clinical practice. The introduction of microbubbles allows localization of the injected material and real-time monitoring of the sonoporation procedure in the treatment site. This method has the potential to be used for many different applications, promoting in situ tissue engineering. In the context of bone fractures, this therapy can be applied to a variety of orthopedic indications. It is minimally invasive, does not require ex vivo stem cell manipulation or the patient's own bone harvest for implantation, and avoids use of costly growth factors. Because no alternative efficient method of inducing bone regeneration in sites with severe bone loss has yet been found, ultrasound-mediated gene therapy is a promising tool that might offer a positive response to this unmet clinical need.

MATERIALS AND METHODS

Study design

The objective of our study was to develop a therapy for critical-sized bone fracture repair consisting of ultrasound-mediated gene targeting to endogenous MSCs. Our prespecified hypothesis was that ultrasound-mediated, microbubble-enhanced gene delivery of *BMP-6* would lead to efficient bone regeneration and fracture healing in a clinically relevant, large animal model. Male and female Yucatán mini-pigs (S&S Farms) were used in this study. The mean weight ± SD of the animals was 37.0 ± 3.6 kg, and their mean age ± SD was 7.8 ± 1.2 months. The sample size used was estimated to achieve a power of 0.8 and $\alpha = 0.05$ using one-way ANOVA.

Sonoporation was investigated for its capacity to regenerate a critical-sized tibial bone fracture. Pigs underwent surgery consisting of the creation of a 1-cm critical-sized bone fracture in the tibia bone. During the same surgery, a collagen scaffold was implanted within the fracture site to recruit endogenous MSCs. Fourteen days later, the pigs were randomly assigned either to receive the treatment, which consisted of an injection of *BMP-6* plasmid

premixed with microbubbles to the fracture site followed by ultrasound application (*BMP-6* + US), or to one of the control groups. The following control groups were used: (i) No treatment (Scaffold only); (ii) *BMP-6* plasmid premixed with micro-bubbles injection (*BMP-6*); or (iii) empty plasmid vector premixed with microbubbles injection followed by ultrasound application (US only). In addition, a control group treated with an autograft (Autograft) was used to assess treatment efficacy compared to the gold-standard treatment for large fractures. Sonoporation potency was estimated using reporter gene expression and tissue analysis for *BMP-6* gene and protein expression. Bone formation was assessed using μCT, histology, and biomechanical testing. Animals that developed acute procedural complications, such as bone fixation failure or signs of distress during follow-up that compromised animal welfare, were eliminated from the study.

Plasmid DNA production

Plasmids encoding luciferase under the control of the ubiquitin promoter (*pUb-Luc2*) and enhanced GFP under the control of the cytomegalovirus promoter (*pCMV-EGFP-N1*) were used to study transgene expression. A plasmid encoding BMP-6 under the control of the cytomegalovirus promoter (*pCMV-BMP6*) was used to induce bone regeneration. Plasmid preparation was detailed elsewhere (58, 59). All plasmids were expanded using standard laboratory procedures and purified using an EndoFree Kit (Qiagen).

Critical-sized tibia fracture model: Surgical procedure

All animal procedures were approved by the Cedars-Sinai Medical Center institutional review board for animal experiments (IACUC #004740). A critical-sized circumferential bone defect of 1 cm in length was created in the tibia bones of Yucatán mini-pigs per previously described method (60). A critical-sized defect in humans was defined as “involving 50% of the cortical diameter of the tibia and >1 cm in length” (61). The average length of the tibia bone in the Yucatán mini-pig is 10 cm, and in an adult human it is 43 cm. Hence, a 1-cm defect in the mini-pig can be compared to a 4.3-cm defect in an average person. After an 18-hour preoperative fast, each mini-pig was sedated using intramuscular acepromazine (0.25 mg/kg), ketamine (20 mg/kg), and atropine (0.02 to 0.05 mg/kg). The animal was then administered propofol (2 mg/kg) intravenously, and endotracheal intubation was performed. Anesthesia was maintained using 1 to 3.5% inhaled isoflurane for the duration of the procedure. A 10-cm anteromedial skin incision was made over the tibia. Soft tissue and periosteum were bluntly dissected to expose the tibial diaphysis. An oscillating saw (CONMED) was used to remove 1 cm of bone and create a segmental bone fracture. The fracture was internally fixated using a custom-made six-hole limited-contact dynamic compression plate (Veterinary Orthopedic Implants; fig. S1), and a flat sheet of biodegradable collagen scaffold (DuraGen Matrix, Integra LifeSciences) with a pore size of 100 μm was shaped and implanted in the fracture site. For autograft-treated animals, the resected bone segment was grafted into the fracture and fixated using the fixation plate. Finally, the subcutaneous tissue was closed with an absorbable subcutaneous suture, and the skin was closed using a nonabsorbable suture, which was removed 2 weeks after surgery. The animal received perioperative antimicrobial prophylaxis (ceftiofur, 0.05 ml/kg) and postoperative analgesia (buprenorphine, 0.2 mg/kg).

Flow cytometry characterization of cells recruited to fracture site

Nine animals underwent surgery and were anesthetized and sacrificed by injection of veterinary euthanasia solution (VetOne) on postoperative days 7, 14, and 21 (three animals were euthanized per time point). Postmortem tissue was extracted from the fracture site, washed with phosphate-buffered saline (PBS), digested using 0.1% collagenase (type 1A, Sigma-Aldrich) for 1 hour, filtrated using a 70-μm cell strainer, and centrifuged at 2000 rpm for 7 min. Freshly isolated cells were analyzed for MSC surface markers, taking into consideration the limited availability of anti-pig antibodies. The cells were stained with mouse anti-human (with cross-reactivity to pig) CD90, mouse anti-pig CD29 (BD Biosciences Pharmingen), and rat anti-pig CD44 (Fitzgerald Industries International). Primary antibodies were detected by applying fluorochrome-conjugated secondary antibodies rat anti-mouse–PE (phycoerythrin) (BD Biosciences Pharmingen) and donkey anti-rat–PE (Imgenex Corp.) according to the manufacturer's recommendations. The cells were analyzed and plotted using an LSR II flow cytometer, BD FACSDiva, and FCS Express software (BD). Nonspecific binding of secondary antibodies was quantified, and the fluorescence signal was subtracted from the detection values of the experimental group.

Ultrasound-mediated, microbubble-enhanced gene delivery

Fourteen days after fracture creation, scaffold implantation, and bone stabilization, each animal was sedated in the manner described above. First, a microbubble suspension (DEFINITY, Lantheus Medical Imaging) composed of a gas core containing octafluoropropane and a lipid shell was activated by 45 s of shaking using a VIALMIX shaker (Lantheus Medical Imaging). Then, 10^7 microbubbles and 1-mg plasmid DNA were mixed together to a final volume of 500 μl. To avoid microbubble aggregation and adhesion to syringe walls, we manually rotated the syringe containing the mixture periodically before injection. Next, the fracture was located using a Fluoroscan mini C-arm (Hologic), and an 18-gauge needle was inserted into the center of the fracture (fig. S3A). The mixture was injected while being visualized using a Sonos 5500 (Philips Ultrasound) unit equipped with a focused S3 probe set to B-mode with its focal point matching the location of the defect (fig. S3, B and C). Then, a therapeutic ultrasonic pulse was applied using cadence contrast agent imaging mode at a transmission frequency of 1.3 MHz, a mechanical index of 0.6, and a depth of 4 cm for about 2 min until microbubble oscillation could no longer be visualized (fig. S3D). Repeated oscillation of the microbubbles eventually results in dissolution as a result of either fragmentation or diffusion (62).

Transfection efficacy evaluation: GFP expression

Six animals underwent surgery. Fourteen days later, the mini-pigs were injected with *GFP* plasmid premixed with microbubbles. The animals were randomly assigned so only half were treated with ultrasound immediately after the injection. Five days after transfection, the animals were sacrificed. Ex vivo optical imaging of the fracture site was performed using a fluorescence imaging system (IVIS; PerkinElmer) to localize the signal within the treated limb. Then, cells from the fracture sites were isolated as described above. The cells were examined using flow cytometry to detect GFP expression. The percentage of GFP-positive cells served as a measure of transfection rate.

Transfection efficacy evaluation: Luciferase expression

Six animals underwent surgery and 14 days later were injected with *luciferase* plasmid premixed with microbubbles. The animals were randomly assigned so only half were treated with ultrasound immediately after the injection. Five days after transfection, cells from the fracture sites were isolated as described above and incubated with luciferase lysis buffer (Promega). The resulting homogenate was centrifuged at 10,000*g* for 10 min, and 100 μl of luciferase reaction buffer (Promega) was added to 20 μl of the clear supernatant. Light emission was measured by a luminometer (TD-20/20; Turner BioSystems) in RLU. The values were normalized for protein content, which was measured using bicinchoninic acid assay (Pierce). Luciferase activity was expressed as RLU per milligram of protein.

BMP-6 gene and protein expression analysis

Eighteen animals underwent surgery and 14 days postoperatively were injected with *BMP-6* plasmid premixed with microbubbles. The animals were randomly assigned so only half were treated with ultrasound immediately after the injection. Then, animals were randomly sacrificed 2, 5, or 10 days after ultrasound transfection. Tissues were collected postmortem to characterize *BMP-6* gene and protein expression.

Quantitative reverse transcription PCRs (RT-PCRs) were performed to quantify *BMP-6* gene expression in various organs after ultrasound transfection. Tissues from the fracture site, brain, bone marrow, lung, liver, heart, skeletal muscle, and spleen were harvested postmortem, and RNA was isolated using an RNeasy extraction kit (Qiagen). The RNA was then reverse-transcribed using random primers and reverse tran-scriptase (Promega). Expression of *BMP-6* gene was analyzed using the ABI 7500 Prism system (Applied Biosystems) with Hs00233470_m1 primer (ABI). 18*S* was used as a housekeeping gene control.

Enzyme-linked immunosorbent assay (ELISA) was used to estimate BMP-6 protein expression in fracture over time. Tissue from the fracture site was homogenized using tissue homogenizer (VWR) and incubated with proteinase inhibitors (Roche) at 4°C for 2 hours. The resulting homogenate was centrifuged at 12,000 rpm for 10 min, and the supernatant was collected for a BMP-6 ELISA assay (R&D Systems). Values were normalized for protein content, which was measured using bicinchoninic acid assay (Pierce).

Bone formation analysis using μCT

Twenty-eight mini-pigs underwent surgery and were randomly assigned to receive the following 14 days later: (i) No treatment (“Scaffold only” group); (ii) *BMP-6* plasmid premixed with microbubbles (“*BMP-6*” group); (iii) empty plasmid vector premixed with microbubbles and ultrasound (“US only” group); (iv) *BMP-6* plasmid premixed with microbubbles and ultrasound (“*BMP-6* + US” group); or (v) autograft implantation (“Autograft” group). Eight weeks postoperatively, the animals were euthanized and their tibiae were harvested for ex vivo, high-resolution μCT (vivaCT 40; SCANCO Medical AG), as previously described (63). Microtomographic slices were acquired using an x-ray tube with a 55-kVp (kilovolt peak) potential and reconstructed at a vox-el size of 35 μm. The fracture was evaluated using histomorphometric three-dimensional (3D) evaluation. A

constrained 3D Gaussian filter (σ = 0.8, support = 1) was used to partly suppress noise in the volume of interest. The bone tissue was segmented from marrow and soft tissue using a global thresholding procedure. A quantitative assessment of bone volume density and apparent density based on micro-tomographic data sets was created using direct 3D morphometry.

Histological evaluation

One specimen from each treatment group was used for histological evaluation. The specimens were cleaned and fixed in 4% formalin for 3 days. Dehydration was accomplished using a graded series of ethyl alcohols and three stages of xylene. Infiltration was performed using a graded series of xylene and Osteo-Bed (Polysciences) resins, followed by a catalyzed mixture of Osteo-Bed resin containing benzoyl peroxide (1.40 g/100 ml). Embedding was performed using a final catalyzed resin mixture of Osteo-Bed resin solution containing benzoyl peroxide (2.5 g/100 ml). Tissue sections were cut at a section thickness of 5.0 μm on aRM2155 rotary microtome(Leica) byusingtungsten carbide D-profile knives. The sections were stained using matrix-specific Masson's trichrome staining. In brief, tissue sections were treated overnight in Bouin's solution at room temperature. Slides were rinsed for 10 min under running water and stained with Weigert's hematoxylin for 5 min. The slides were then rinsed and stained with scarlet-acid fuchsin for 5 min and rinsed again, after which the slides were again stained with phosphomolybdic-phosphotungstic, aniline blue, and 2% acetic acid for 5 min each. Finally, the slides were rinsed, dried, and mounted. The slides were imaged using a four-channel Laser Scanning Microscope 780 (Zeiss) with ×20 magnification, z-stacking, and 5 × 5 tile scanning. For zoom-in images, a single z-stacked image was generated. All samples were scanned using the same gain and exposure settings.

Biomechanical analysis

Fifteen samples from the "Autograft," "*BMP-6* + US," and "*BMP-6* only" groups (n = 5 per group) were used for biomechanical analysis. After harvest, the samples were wrapped in saline-soaked gauze, sealed, and frozen until analysis. Before analysis, the samples were thawed for about 1 hour and then allowed to rehydrate in PBS for 2 hours. A custom-made alignment jig was used to fix the proximal and distal ends of the tibia in two aluminum square pots by submerging 2.5 cm of each end in Bosworth Fastray Cement (Midway Dental Supply). The gauge length of the exposed tibia between the two fixed ends was measured using calipers before testing. Torsion testing was performed using a custom-designed jig on an Instron ElectroPuls E10000 (Instron). The rotational actuator was rotated at a rate of 1 deg/s until failure. Load and rotation data were continuously recorded during testing. The collected data were analyzed using a custom MATLAB code (data file S1) to determine the torsional rigidity, yield torque, ultimate torque, rotation-to-yield torque, rotation-to-ultimate torque, work-to-yield torque, and work-to-ultimate torque.

Statistical analysis

GraphPad Prism 5.0f software (GraphPad Prism) was used to analyze the data. Results are presented as means ± SEM. Data analysis was conducted using Student's *t* test, one-way ANOVA, or a two-way ANOVA with Tukey's multiple comparison post hoc test. To assess

significance, we considered $P < 0.05$ statistically significant. Individual-level data are shown in table S1.

Acknowledgments

We thank S. De Mel for the dedicated laboratory work during this study.

Funding: We acknowledge funding from California Institute for Regenerative Medicine (CIRM) grant TR4-06713, a grant from IDF Medical Corps, a grant from Milgrom Family (D.G.), NIH R01CA112356 (K.W.F.), and NIH P30AR069655 (H.A.A.).

REFERENCES AND NOTES

1. Hak DJ, Fitzpatrick D, Bishop JA, Marsh JL, Tilp S, Schnettler R, Simpson H, Alt V. Delayed union and nonunions: Epidemiology, clinical issues, and financial aspects. Injury. 2014; 45(Suppl 2):S3–S7.
2. Awad HA, Zhang X, Reynolds DG, Guldberg RE, O'Keefe RJ, Schwarz EM. Recent advances in gene delivery for structural bone allografts. Tissue Eng. 2007; 13:1973–1985. [PubMed: 17518728]
3. Bishop JA, Palanca AA, Bellino MJ, Lowenberg DW. Assessment of compromised fracture healing. J Am Acad Orthop Surg. 2012; 20:273–282. [PubMed: 22553099]
4. Hierholzer C, Sama D, Toro JB, Peterson M, Helfet DL. Plate fixation of ununited humeral shaft fractures: Effect of type of bone graft on healing. J Bone Joint Surg Am. 2006; 88:1442–1447. [PubMed: 16818968]
5. Brigman BE, Hornicek FJ, Gebhardt MC, Mankin HJ. Allografts about the knee in young patients with high-grade sarcoma. Clin Orthop Relat Res. 2004; 421:232–239.
6. Govender S, Csimma C, Genant HK, Valentin-Opran A, Amit Y, Arbel R, Aro H, Atar D, Bishay M, Borner MG, Chiron P, Choong P, Cinats J, Courtenay B, Feibel R, Geulette B, Gravel C, Haas N, Raschke M, Hammacher E, van der Velde D, Hardy P, Holt M, Josten C, Ketterl RL, Lindeque B, Lob G, Mathevon H, McCoy G, Marsh D, Miller R, Munting E, Oevre S, Nordsletten L, Patel A, Pohl A, Rennie W, Reynders P, Rommens PM, Rondia J, Rossouw WC, Daneel PJ, Ruff S, Ruter A, Santavirta S, Schildhauer TA, Gekle C, Schnettler R, Segal D, Seiler H, Snowdowne RB, Stapert J, Taglang G, Verdonk R, Vogels L, Weckbach A, Wentzensen A, Wisniewski T. BMP-2 Evaluation in Surgery for Tibial Trauma (BESTT) Study Group. Recombinant human bone morphogenetic protein-2 for treatment of open tibial fractures: A prospective, controlled, randomized study of four hundred and fifty patients. J Bone Joint Surg Am. 2002; 84:2123–2134. [PubMed: 12473698]
7. Ristiniemi J, Flinkkilä T, Hyvönen P, Lakovaara M, Pakarinen H, Jalovaara P. RhBMP-7 accelerates the healing in distal tibial fractures treated by external fixation. J Bone Joint Surg Br. 2007; 89:265–272. [PubMed: 17322450]
8. Carragee EJ, Hurwitz EL, Weiner BK. A critical review of recombinant human bone morphogenetic protein-2 trials in spinal surgery: Emerging safety concerns and lessons learned. Spine J. 2011; 11:471–491. [PubMed: 21729796]
9. Bleich NK, Kallai I, Lieberman JR, Schwarz EM, Pelled G, Gazit D. Gene therapy approaches to regenerating bone. Adv Drug Deliv Rev. 2012; 64:1320–1330. [PubMed: 22429662]
10. Betz OB, Betz VM, Nazarian A, Egermann M, Gerstenfeld LC, Einhorn TA, Vrahas MS, Bouxsein ML, Evans CH. Delayed administration of adenoviral BMP-2 vector improves the formation of bone in osseous defects. Gene Ther. 2007; 14:1039–1044. [PubMed: 17460719]
11. Egermann M, Lill CA, Griesbeck K, Evans CH, Robbins PD, Schneider E, Baltzer AW. Effect of BMP-2 gene transfer on bone healing in sheep. Gene Ther. 2006; 13:1290–1299. [PubMed: 16642029]
12. Yazici C, Takahata M, Reynolds DG, Xie C, Samulski RJ, Samulski J, Beecham EJ, Gertzman AA, Spilker M, Zhang X, O'Keefe RJ, Awad HA, Schwarz EM. Self-complementary AAV2.5-BMP2-coated femoral allografts mediated superior bone healing versus live autografts in mice with equivalent biomechanics to unfractured femur. Mol Ther. 2011; 19:1416–1425. [PubMed: 21206485]

13. Trono D. Gene therapy: Too much splice can spoil the dish. J Clin Invest. 2012; 122:1600–1602. [PubMed: 22523063]
14. Kimelman-Bleich N, Pelled G, Zilberman Y, Kallai I, Mizrahi O, Tawackoli W, Gazit Z, Gazit D. Targeted gene-and-host progenitor cell therapy for nonunion bone fracture repair. Mol Ther. 2011; 19:53–59. [PubMed: 20859259]
15. Sheyn D, Kimelman-Bleich N, Pelled G, Zilberman Y, Gazit D, Gazit Z. Ultrasound-based nonviral gene delivery induces bone formation in vivo. Gene Ther. 2008; 15:257–266. [PubMed: 18033309]
16. Shapiro G, Wong AW, Bez M, Yang F, Tam S, Even L, Sheyn D, Ben-David S, Tawackoli W, Pelled G, Ferrara KW, Gazit D. Multiparameter evaluation of in vivo gene delivery using ultrasound-guided, microbubble-enhanced sonoporation. J Control Release. 2016; 223:157–164. [PubMed: 26682505]
17. Endoh M, Koibuchi N, Sato M, Morishita R, Kanzaki T, Murata Y, Kaneda Y. Fetal gene transfer by intrauterine injection with microbubble-enhanced ultrasound. Mol Ther. 2002; 5:501–508. [PubMed: 11991740]
18. Taniyama Y, Tachibana K, Hiraoka K, Aoki M, Yamamoto S, Matsumoto K, Nakamura T, Ogihara T, Kaneda Y, Morishita R. Development of safe and efficient novel nonviral gene transfer using ultrasound: Enhancement of transfection efficiency of naked plasmid DNA in skeletal muscle. Gene Ther. 2002; 9:372–380. [PubMed: 11960313]
19. Sanches PG, Mühlmeister M, Seip R, Kaijzel E, Löwik C, Bohmer M, Tiemann K, Grüll H. Ultrasound-mediated gene delivery of naked plasmid DNA in skeletal muscles: A case for bolus injections. J Control Release. 2014; 195:130–137. [PubMed: 24979212]
20. Watanabe Y, Horie S, Funaki Y, Kikuchi Y, Yamazaki H, Ishii K, Mori S, Vassaux G, Kodama T. Delivery of Na/I symporter gene into skeletal muscle using nanobubbles and ultrasound: Visualization of gene expression by PET. J Nucl Med. 2010; 51:951–958. [PubMed: 20484436]
21. Li T, Tachibana K, Kuroki M, Kuroki M. Gene transfer with echo-enhanced contrast agents: Comparison between Albunex, Optison, and Levovist in mice—Initial results. Radiology. 2003; 229:423–428. [PubMed: 14512507]
22. Lu QL, Liang HD, Partridge T, Blomley MJ. Microbubble ultrasound improves the efficiency of gene transduction in skeletal muscle in vivo with reduced tissue damage. Gene Ther. 2003; 10:396–405. [PubMed: 12601394]
23. Wang X, Liang HD, Dong B, Lu QL, Blomley MJ. Gene transfer with microbubble ultrasound and plasmid DNA into skeletal muscle of mice: Comparison between commercially available microbubble contrast agents. Radiology. 2005; 237:224–229. [PubMed: 16081853]
24. Shapiro G, Kallai I, Sheyn D, Tawackoli W, Do Koh Y, Bae H, Trietel T, Goldbart R, Kost J, Gazit Z, Gazit D, Pelled G. Ultrasound-mediated transgene expression in endogenous stem cells recruited to bone injury sites. Polym Adv Technol. 2014; 25:525–531.
25. Feichtinger GA, Hofmann AT, Slezak P, Schuetzenberger S, Kaipel M, Schwartz E, Neef A, Nomikou N, Nau T, van Griensven M, McHale AP, Redl H. Sonoporation increases therapeutic efficacy of inducible and constitutive *BMP2/7* in vivo gene delivery. Hum Gene Ther Methods. 2013; 25:57–71. [PubMed: 24164605]
26. Tai K, Pelled G, Sheyn D, Bershteyn A, Han L, Kallai I, Zilberman Y, Ortiz C, Gazit D. Nanobiomechanics of repair bone regenerated by genetically modified mesenchymal stem cells. Tissue Eng Part A. 2008; 14:1709–1720. [PubMed: 18620480]
27. Osawa K, Okubo Y, Nakao K, Koyama N, Bessho K. Osteoinduction by microbubble-enhanced transcutaneous sonoporation of human bone morphogenetic protein-2. J Gene Med. 2009; 11:633–641. [PubMed: 19396932]
28. Bonadio J, Smiley E, Patil P, Goldstein S. Localized, direct plasmid gene delivery in vivo: Prolonged therapy results in reproducible tissue regeneration. Nat Med. 1999; 5:753–759. [PubMed: 10395319]
29. Egermann M, Baltzer AW, Adamaszek S, Evans C, Robbins P, Schneider E, Lill CA. Direct adenoviral transfer of bone morphogenetic protein-2 cDNA enhances fracture healing in osteoporotic sheep. Hum Gene Ther. 2006; 17:507–517. [PubMed: 16716108]

30. Dai KR, Xu XL, Tang TT, Zhu ZA, Yu CF, Lou JR, Zhang XL. Repairing of goat tibial bone defects with BMP-2 gene–modified tissue-engineered bone. Calcif Tissue Int. 2005; 77:55–61. [PubMed: 16007479]
31. Xu XL, Tang T, Dai K, Zhu Z, Guo XE, Yu C, Lou J. Immune response and effect of adenovirus-mediated human BMP-2 gene transfer on the repair of segmental tibial bone defects in goats. Acta Orthop. 2005; 76:637–646. [PubMed: 16263609]
32. Raper SE, Chirmule N, Lee FS, Wivel NA, Bagg A, Gao G-p, Wilson JM, Batshaw ML. Fatal systemic inflammatory response syndrome in a ornithine transcarbamylase deficient patient following adenoviral gene transfer. Mol Genet Metab. 2003; 80:148–158. [PubMed: 14567964]
33. Baum C, Kustikova O, Modlich U, Li Z, Fehse B. Mutagenesis and oncogenesis by chromosomal insertion of gene transfer vectors. Hum Gene Ther. 2006; 17:253–263. [PubMed: 16544975]
34. Hacein-Bey-Abina S, von Kalle C, Schmidt M, Le Deist F, Wulffraat N, McIntyre E, Radford I, Villeval JL, Fraser CC, Cavazzana-Calvo M, Fischer A. A serious adverse event after successful gene therapy for X-linked severe combined immunodeficiency. N Engl J Med. 2003; 348:255–256. [PubMed: 12529469]
35. Busse JW, Bhandari M, Einhorn TA, Schemitsch E, Heckman JD, Tornetta P III, Leung KS, Heels-Ansdell D, Makosso-Kallyth S, Della Rocca GJ, Jones CB, Guyatt GH. TRUST Investigators writing group. Re-evaluation of low intensity pulsed ultrasound in treatment of tibial fractures (TRUST): Randomized clinical trial. BMJ. 2016; 355:i5351. [PubMed: 27797787]
36. Hiremath GK, Steinmetz MP, Krishnaney AA. Is it safe to use recombinant human bone morphogenetic protein in posterior cervical fusion? Spine. 2009; 34:885–889. [PubMed: 19531997]
37. Kang JD. Another complication associated with rhBMP-2? Spine J. 2011; 11:517–519. [PubMed: 21612984]
38. Carragee EJ, Mitsunaga KA, Hurwitz EL, Scuderi GJ. Retrograde ejaculation after anterior lumbar interbody fusion using rhBMP-2: A cohort controlled study. Spine J. 2011; 11:511–516. [PubMed: 21612985]
39. Miyaji H, Sugaya T, Kato K, Kawamura N, Tsuji H, Kawanami M. Dentin resorption and cementum-like tissue formation by bone morphogenetic protein application. J Periodontal Res. 2006; 41:311–315. [PubMed: 16827725]
40. Cowan CM, Aalami OO, Shi Y-Y, Chou YF, Mari C, Thomas R, Quarto N, Nacamuli RP, Contag CH, Wu B, Longaker MT. Bone morphogenetic protein 2 and retinoic acid accelerate in vivo bone formation, osteoclast recruitment, and bone turnover. Tissue Eng. 2005; 11:645–658. [PubMed: 15869441]
41. Little DG, McDonald M, Bransford R, Godfrey CB, Amanat N. Manipulation of the anabolic and catabolic responses with OP-1 and zoledronic acid in a rat critical defect model. J Bone Miner Res. 2005; 20:2044–2052. [PubMed: 16234978]
42. Lavery K, Swain P, Falb D, Alaoui-Ismaili MH. BMP-2/4 and BMP-6/7 differentially utilize cell surface receptors to induce osteoblastic differentiation of human bone marrow-derived mesenchymal stem cells. J Biol Chem. 2008; 283:20948–20958. [PubMed: 18436533]
43. Li JZ, Li H, Sasaki T, Holman D, Beres B, Dumont RJ, Pittman DD, Hankins GR, Helm GA. Osteogenic potential of five different recombinant human bone morphogenetic protein adenoviral vectors in the rat. Gene Ther. 2003; 10:1735–1743. [PubMed: 12939640]
44. Jane JA Jr, Dunford BA, Kron A, Pittman DD, Sasaki T, Li JZ, Li H, Alden TD, Dayoub H, Hankins GR, Kallmes DF, Helm GA. Ectopic osteogenesis using adenoviral bone morphogenetic protein (BMP)-4 and BMP-6 gene transfer. Mol Ther. 2002; 6:464–470. [PubMed: 12377187]
45. Jung Y, Song J, Shiozawa Y, Wang J, Wang Z, Williams B, Havens A, Schneider A, Ge C, Franceschi RT, McCauley LK, Krebsbach PH, Taichman RS. Hematopoietic stem cells regulate mesenchymal stromal cell induction into osteoblasts thereby participating in the formation of the stem cell niche. Stem Cells. 2008; 26:2042–2051. [PubMed: 18499897]
46. Vukicevic S, Grgurevic L. BMP-6 and mesenchymal stem cell differentiation. Cytokine Growth Factor Rev. 2009; 20:441–448. [PubMed: 19900832]

47. Mizrahi O, Sheyn D, Tawackoli W, Kallai I, Oh A, Su S, Da X, Zarrini P, Cook-Wiens G, Gazit D, Gazit Z. BMP-6 is more efficient in bone formation than BMP-2 when overexpressed in mesenchymal stem cells. Gene Ther. 2013; 20:370–377. [PubMed: 22717741]
48. Nomikou N, Feichtinger GA, Saha S, Nuernberger S, Heimel P, Redl H, McHale AP. Ultrasound-responsive gene-activated matrices (GAMs) for osteogenic gene therapy using matrix-assisted sonoporation (MAS). J Tissue Eng Regen Med. 2017
49. Flierl MA, Smith WR, Mauffrey C, Irgit K, Williams AE, Ross E, Peacher G, Hak DJ, Stahel PF. Outcomes and complication rates of different bone grafting modalities in long bone fracture nonunions: A retrospective cohort study in 182 patients. J Orthop Surg Res. 2013; 8:33. [PubMed: 24016227]
50. Friedlaender GE. Bone grafts. The basic science rationale for clinical applications. J Bone Joint Surg Am. 1987; 69:786–790. [PubMed: 3298264]
51. Weiland AJ, Phillips TW, Randolph MA. Bone grafts: A radiologic, histologic, and biomechanical model comparing autografts, allografts, and free vascularized bone grafts. Plast Reconstr Surg. 1984; 74:368–379. [PubMed: 6382367]
52. Peltola MJ, Aitasalo KM, Suonpaa JT, Yli-Urpo A, Laippala PJ. In vivo model for frontal sinus and calvarial bone defect obliteration with bioactive glass S53P4 and hydroxyapatite. J Biomed Mater Res. 2001; 58:261–269. [PubMed: 11319739]
53. Runyan CM, Vu AT, Rumburg A, Bove K, Racadio J, Billmire DA, Taylor JA. Repair of a critical porcine tibial defect by means of allograft revitalization. Plast Reconstr Surg. 2015; 136:461e–473e.
54. Delalande A, Bureau MF, Midoux P, Bouakaz A, Pichon C. Ultrasound-assisted microbubbles gene transfer in tendons for gene therapy. Ultrasonics. 2010; 50:269–272. [PubMed: 19857885]
55. Stephens DN, Kruse DE, Qin S, Ferrara KW. Design aspects of focal beams from high-intensity arrays. IEEE Trans Ultrason Ferroelectr Freq Control. 2011; 58:1590–1602. [PubMed: 21859578]
56. Qin S, Caskey CF, Ferrara KW. Ultrasound contrast microbubbles in imaging and therapy: Physical principles and engineering. Phys Med Biol. 2009; 54:R27–R57. [PubMed: 19229096]
57. Sheyn D, Ben-David S, Shapiro G, De Mel S, Bez M, Ornelas L, Sahabian A, Sareen D, Da X, Pelled G, Tawackoli W, Liu Z, Gazit D, Gazit Z. Human induced pluripotent stem cells differentiate into functional mesenchymal stem cells and repair bone defects. Stem Cells Transl Med. 2016; 5:1447–1460. [PubMed: 27400789]
58. Mizrahi O, Sheyn D, Tawackoli W, Kallai I, Oh A, Su S, Da X, Zarrini P, Cook-Wiens G, Gazit D, Gazit Z. BMP-6 is more efficient in bone formation than BMP-2 when overexpressed in mesenchymal stem cells. Gene Ther. 2012; 20:370–377. [PubMed: 22717741]
59. Sheyn D, Kallai I, Tawackoli W, Yakubovich DC, Oh A, Su S, Da X, Lavi A, Kimelman-Bleich N, Zilberman Y, Li N, Bae H, Gazit Z, Pelled G, Gazit D. Gene-modified adult stem cells regenerate vertebral bone defect in a rat model. Mol Pharm. 2011; 8:1592–1601. [PubMed: 21834548]
60. Raschke M, Kolbeck S, Bail H, Schmidmaier G, Flyvbjerg A, Lindner T, Dahne M, Roenne IA, de Haas NDH. Homologous growth hormone accelerates healing of segmental bone defects. Bone. 2001; 29:368–373. [PubMed: 11595620]
61. Court-Brown, C-M., Bucholz, RW., Heckman, JD. Rockwood and Green's Fractures in Adults. 6. Lippincott Williams and Wilkins; 2005. Fractures of the tibia and fibula; p. 2079-2146.
62. Chomas JE, Dayton P, Allen J, Morgan K, Ferrara KW. Mechanisms of contrast agent destruction. IEEE Trans Ultrason Ferroelectr Freq Control. 2001; 48:232–248. [PubMed: 11367791]
63. Sheyn D, Shapiro G, Tawackoli W, Jun DS, Koh Y, Kang KB, Su S, Da X, Ben-David S, Bez M, Yalon E, Antebi B, Avalos P, Stern T, Zelzer E, Schwarz EM, Gazit Z, Pelled G, Bae HM, Gazit D. PTH induces systemically administered mesenchymal stem cells to migrate to and regenerate spine injuries. Mol Ther. 2016; 24:318–330.

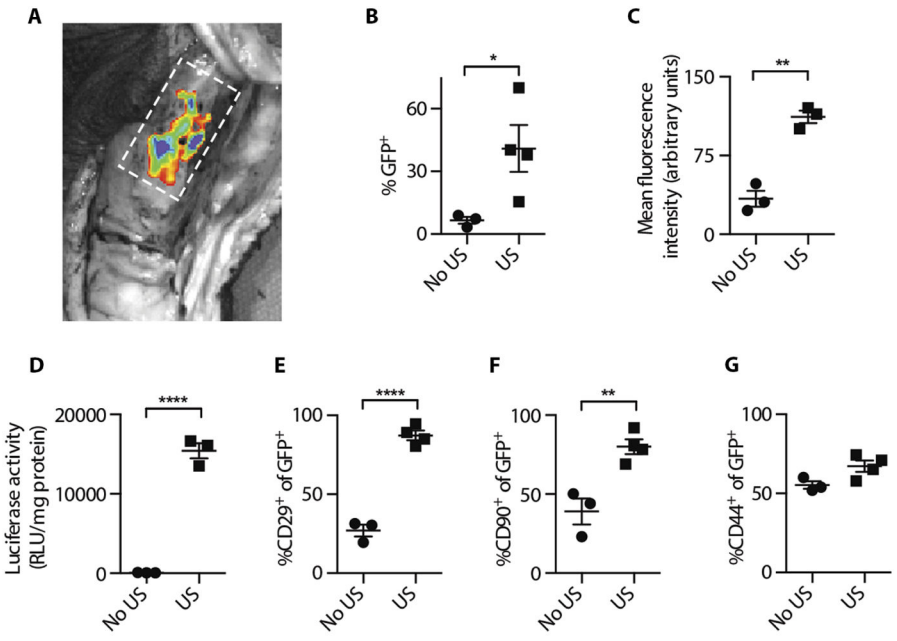

Fig. 1. Reporter gene expression in mini-pig tibial fractures after ultrasound-mediated gene delivery

(**A**) Ex vivo fluorescence imaging of an exposed *GFP*-treated fracture 5 days after treatment. Fracture margins are represented by a dashed rectangle. (**B**) Flow cytometry analysis of the percentage of GFP^+ cells isolated from fracture sites 5 days after treatment with or without ultrasound (*$P = 0.049$). (**C**) Mean fluorescence intensity per cell isolated from fractures 5 days after treatment with or without ultrasound (**$P = 0.0013$). (**D**) Luciferase enzyme activity in cells isolated from fracture sites 5 days after treatment with or without ultrasound (****$P = 0.0001$). Percentage of (**E**) $CD29^+$ (****$P = 0.0001$), (**F**) $CD90^+$ (**$P = 0.0057$), and (**G**) $CD44^+$ cells ($P = 0.0531$) out of GFP^+ cells isolated from fractures 5 days after treatment with or without ultrasound. Data are means ± SEM; *P* values were determined by two-tailed Student's *t* tests (No US, $n = 3$; US, $n = 4$; RLU, relative light units).

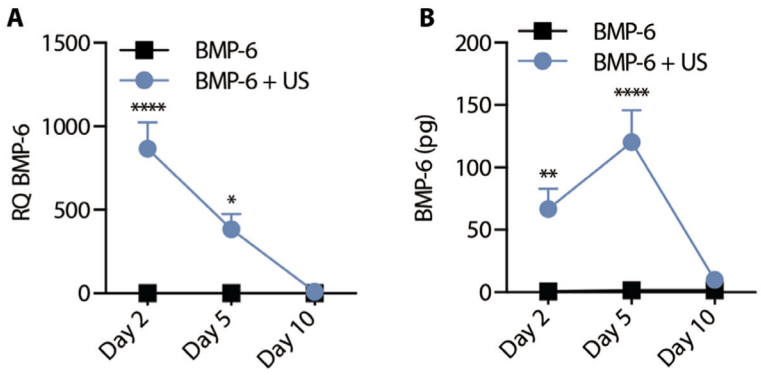

Fig. 2. *BMP-6* expression after ultrasound-mediated gene delivery to tibia fractures in mini-pigs

(**A**) Gene [relative quantification (RQ); **P* = 0.0111, *****P* = 0.0001] and (**B**) protein expression (***P* = 0.0085, *****P* = 0.0001) in tibial fracture sites 2, 5, and 10 days after ultrasound-mediated *BMP-6* gene delivery. Data are means ± SEM; *P* values were determined by two-way analysis of variance (ANOVA) with multiple comparisons (*n* = 3 per experimental group).

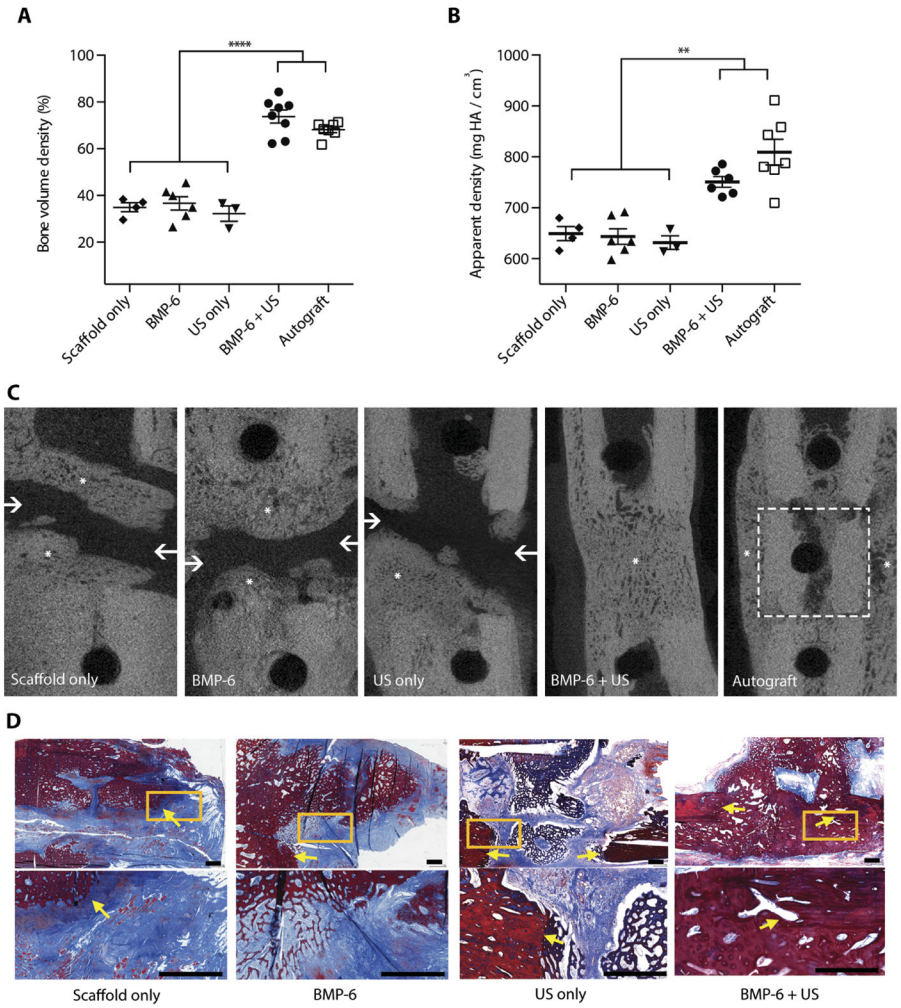

Fig. 3. Ultrasound-mediated *BMP-6* gene delivery to mini-pig tibial bone fractures

Quantitative analysis of bone formation in the tibial fractures, including (**A**) bone volume density (**** $P = 0.0001$) and (**B**) apparent density (** $P = 0.0029$). Data are means ± SEM; P values were determined by one-way ANOVA with multiple comparisons. (**C**) Representative μCT slices of the fractures 8 weeks after surgery. Asterisks represent new bone formation within the fracture. Arrows point to cortical discontinuity indicating nonunion within the fracture. Autograft margins are represented by a dashed square. (**D**) Masson's trichrome staining of tibial fractures 8 weeks after surgery at low magnification (upper subfigures) and high magnification of the yellow square (lower subfigures). Arrows point to the border between native bone and newly formed bone in the fracture. Scale bars, 1 mm. (Autograft, $n = 7$; BMP-6 + US, $n = 8$; BMP-6, $n = 6$; US only, $n = 3$; Scaffold only, $n = 4$; HA, hydroxyapatite.)

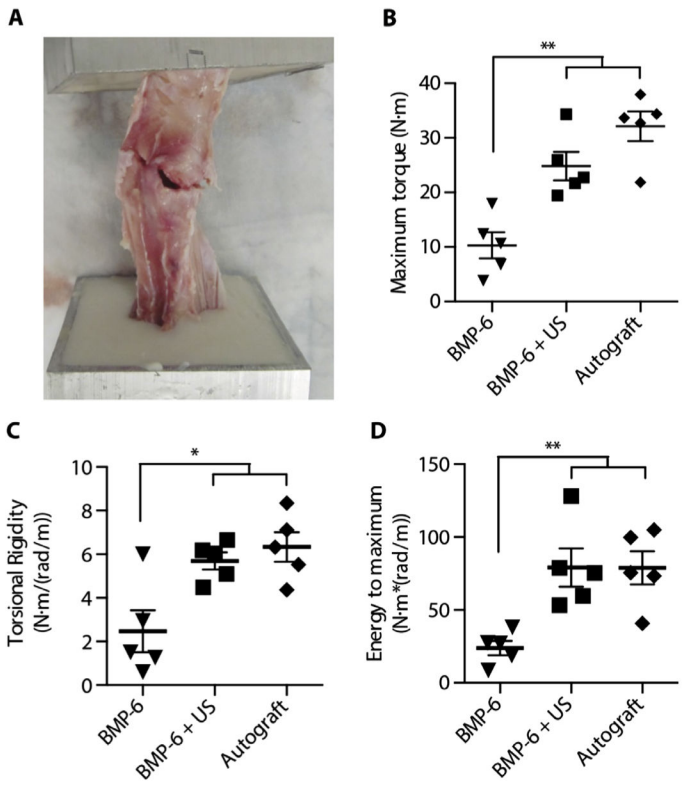

Fig. 4. Biomechanical properties of treated tibiae

Torsion testing was performed on tibiae harvested from treated mini-pigs. (**A**) Photograph of a tibia reaching its failure point during biomechanical testing. Analysis of load and rotation was performed to determine the (**B**) maximum torque (strength; $^{**}P = 0.0048$), (**C**) torsional rigidity (stiffness; $^{*}P = 0.02$), and (**D**) energy to maximum (toughness; $^{**}P = 0.0077$) of treated bones. Data are means ± SEM; *P* values were determined by one-way ANOVA with multiple comparisons (N·m, Newton meter; $n = 5$ per experimental group).